Laser and Particle Beams (2007), *25*, 397–406. Printed in the USA.

DOI: 10.1017/S0263034607000511

Oscillating two stream instability of a plasma wave in a negative ion containing plasma with hot and cold positive ions

HITENDRA K. MALIK

Plasma Waves and Particle Acceleration Laboratory, Department of Physics, Indian Institute of Technology Delhi, New Delhi, India

(Received 3 February 2007; Accepted 7 May 2007)

Abstract

An oscillating two-stream instability (OTSI) is investigated in plasma, which has hot and cold positive ions, negative ions, and the electrons. For this, a long wavelength plasma wave is considered to be driven by two copropagating lasers with frequencies ω_{L1} and ω_{L2}, such that their difference is almost equal to the electron plasma frequency ω_p. In the present mechanism, this plasma beat wave (ω_b, k_b) is taken to grow in amplitude, so that it becomes susceptible to the OTSI and produces a low frequency electrostatic mode (ω, k), and two shorter wavelength Langmuir wave sidebands (ω_1, k_1) and (ω_2, k_2) with $\omega_1 = \omega - \omega_b$, $\omega_2 = \omega + \omega_b$, $k_1 = k - k_b$, and $k_2 = k + k_b$ in the plasma. The effects of charge number Z, mass, temperature, and density of the ions are studied on the growth rate of the instability, and the amplitudes and phases of the sideband waves generated during the OTSI. It is found that the effects of charge number and mass of the ions are significant on the instability.

Keywords: Oscillating two stream instability; Laser driven plasma wave; Growth rate; Sideband waves

1. INTRODUCTION

Due to diverse applications of the subject particle acceleration, both experimental and theoretical investigations have been made all over the world, and various schemes have been proposed and employed for achieving effective electron acceleration (Nishida & Sato, 1987; Nishida & Shinozaki, 1990; Nakajima, 1996; Umstadter, 2001; Balakirev *et al.*, 2001; Joshi *et al.*, 2002; Reitsma & Jaroszynski, 2004; Katsouleas, 2004; Baiwen *et al.*, 2004; Kawata *et al.*, 2005; Sakai *et al.*, 2006; Koyama *et al.*, 2006; Lifschitz *et al.*, 2006; Flippo *et al.*, 2007; Gupta & Suk, 2007; Kumar *et al.*, 2006). With the help of three-dimensional (3D) particle simulation, Kawata *et al.* (2005) have studied the trapping of electron bunch and its acceleration by the ponderomotive force of a short pulsed laser of TEM (1, 0) + TEM (0, 1) mode. Baiwen *et al.* (2004) have investigated the electron acceleration by an intense laser pulse in low density plasma and observed a short high quality well collimated relativistic electron beam in the direction opposite to the laser propagation. Lifschitz et al. (2006) have proposed a design of a two stage compact GeV electron accelerator. Kumar *et al.* (2006) have studied the effect of a relativistically intense Gaussian laser pulse on the propagation of electron plasma wave, and particle acceleration via modified coupled equations for the laser and electron plasma wave. Recently, Flippo *et al.* (2007) have shown in a laser driven ion accelerator that the spectral shape of the accelerated particles can be controlled, to yield a range of distribution, from Maxwellian to ones possessing a monoenergetic peak at high energy. Further, based on numerical modeling, they have identified a new acceleration mechanism, the laser breakout afterburner, which could potentially boost particle energies by up to two orders of magnitude for the same laser parameters. In addition, efforts have been made related to wakefield excitation by relativistic electron bunch (Balakirev *et al.*, 2001), by different shapes of laser pulses (Kumar *et al.*, 2006), and coupling of longitudinal and transverse motion of accelerated electrons in laser wakefield (Reitsma & Jaroszynski, 2004).

An outstanding application of intense accelerated particle beams is in inertial fusion, different aspects of which have been discussed by several authors (Blazquez, 2002; Davidson *et al.*, 2002; Barnard *et al.*, 2003; Kawata *et al.*,

Address Correspondence and reprint requests to: Hitendra K. Malik, Plasma Waves and Particle Acceleration Laboratory, Department of Physics, Indian Institute of Technology Delhi, New Delhi -- 110 016, India. E-mail: hkmalik@physics.iitd.ac.in; hkmalik@hotmail.com

2003; Hora, 2004; Li *et al.*, 2004; Leon *et al.*, 2005; Kilkenny *et al.*, 2005; Hoffmann *et al.*, 2005; Perlado *et al.*, 2005; Imasaki & Li, 2007). In order to realize an efficient stable beam transport, beam focusing and uniform fuel pellet implosion, Kawata *et al.* (2003) have proposed to use an insulator annular tube guide at the final transport part through which a heavy ion beam is transported. Kilkenny *et al.* (2005) have discussed the target designs, particularly laser targets, which were shown to compensate the limitations in inertial confinement fusion drivers (Koresheva *et al.*, 2005). Li *et al.* (2004) have derived the features of the astrophysical S-function in terms of models related to d + d fusion and d + ^{3}He fusion. Blazquez (2002) has investigated the application of solitons to the study of laser propagation into thermonuclear plasma in inertial confinement fusion. Recently, Imasaki and Li (2007) have discussed an approach for producing efficient and economical hydrogen through a fusion reactor, with the application of magnetic field such that neutrons and charged particles from nuclear reactions are separated from each other by this magnetic field. On the other hand, in such inertial fusion related plasmas or during interaction of high intensity lasers with plasmas, some instability arise due to the perturbation of unstable equilibrium states, which have been investigated by several researchers (Oron *et al.*, 1999; Qin *et al.*, 2003; Rudraiah *et al.*, 2004; Bret *et al.*, 2005, 2006, 2007; Bret & Deutsch, 2006). In addition, other types of instabilities have been studied in different types of plasma models (Nejoh, 1992; Pajouh *et al.*, 2004; Starodubtsev *et al.*, 2004, 2006).

In most of the schemes discussed above for the particle acceleration, the main requirement for attaining greater acceleration is the larger amplitude of the plasma wave. However, the amplitude of the plasma wave cannot be raised indefinitely, as there is a limit of the field that can be supported by plasma. Moreover, when the plasma wave amplitude becomes sufficiently large, it becomes susceptible to the oscillating two-stream instability (OTSI). In the OTSI, a long wavelength pump wave (or plasma wave) near the critical layer excites a short wavelength standing Langmuir wave, and a purely growing density perturbation. In the region where the electric field of the pump and Langmuir waves are parallel, the plasma is pushed away to the region where the fields are antiparallel. Then the depressed density region attracts electric field energy from the neighborhood that leads to deeper density depression and enhancement of the short wavelength Langmuir wave (Liu & Kaw, 1976; Kruer, 1987).

There has been a significant interest in two ion species plasmas in addition to the ordinary plasmas having positive ions and the electrons, as they resemble hohlraum plasmas encountered in indirect drive fusion (Kirkwood *et al.*, 1996; Fernandez *et al.*, 1996; Young *et al.*, 1996; Kuzora *et al.*, 2001). Kirkwood *et al.* (1996) have experimentally studied the stimulated Raman scattering (SRS) and stimulated Brillouin scattering (SBS) from Xe plasma embedded with C_5H_{12} impurities, and found that the ion wave damping is varied in well-characterized plasma with the concentration of C_5H_{12} impurity. In addition, the reflectivity of SRS was found to increase with the concentration of the dopant, which demonstrated the effect of ion wave damping on SRS. Fernandez *et al.* (1996) have observed the dependence of SRS on ion acoustic damping in hohlraum plasmas. They showed that the reflectivity of a laser due to SRS from long scale length hohlraum plasmas depends on the damping of ion-acoustic waves; this dependence was observed particularly in the plasmas with either low or high ionization states. The thresholds of the SBS instability and the nonlinear influence of the driving field on the SBS spectrum have been studied in plasmas with two ion species (Kuzora *et al.*, 2001). In addition, Satya *et al.* (1985) have treated the problem of plasma having two ion species and obtained extensive analytical reductions of the low frequency dispersion relation of the field plasma system, including results on the oscillating two-stream instability.

Since there is an increasing interest, in the research community, in multiple species plasmas and the OTSI of an electrostatic wave is an important issue in nonlinear plasma physics (Nishikawa, 1968*a*, 1968*b*; Nicholson, 1981; Mulser *et al.*, 1984; Gupta *et al.*, 2004; Kumar & Malik, 2006), the instability of a laser driven plasma beat wave has been studied in the present paper, considering a plasma with hot and cold positive ions, negative ions, and the electrons. Here the growth rate of the instability and the behavior of amplitudes and phases of the sidebands generated during the OTSI are studied in great detail.

2. OSCILLATING TWO STREAM INSTABILITY: GROWTH RATE

A homogeneous plasma is considered, which has the electrons (density n_e, mass m_e, and temperature T_e), hot positive ions (density n_h, mass m_h, and temperature T_h) and cold positive ions (density n_c, mass m_c, and temperature T_c), and negative ions (density n_n, mass m_n, and temperature T_n). The same approach as used by Gupta *et al.* (2004) is followed and two collinear laser beams of the amplitudes $\vec{E}_{L1} = \hat{x}A_{L1}e^{-i(\omega_{L1}t-k_{L1}z)}$ and $\vec{E}_{L2} = \hat{x}A_{L2}e^{-i(\omega_{L2}t-k_{L2}z)}$ are considered to propagate through the plasma together with ω_{L1} and ω_{L2} as their frequencies such that $\omega_{L1} - \omega_{L2} \approx \omega_p$, $\omega_{L1,L2} > \omega_p$ and k_{L1} and k_{L2} as their wave vectors. The oscillatory velocities of the electrons produced by the lasers are given by $\vec{v}_{L1} = e\vec{E}_{L1}/m_e i\omega_{L1}$ and $\vec{v}_{L2} = e\vec{E}_{L2}/m_e i\omega_{L2}$, and the exerted ponderomotive force $\vec{F}_p = -(e/2c)\vec{v}_{L1} \times \vec{B}^*_{L2} + \vec{v}^*_{L2} \times \vec{B}_{L1}) = \hat{z}iek_b\phi_{pL}$ together with $\phi_{pL} = -(m_e/2e)\vec{v}_{L1} \cdot \vec{v}^*_{L2}) = \phi_{pL}e^{-i(\omega_b t-k_b z)}$. Here $\omega_b = \omega_{L1} - \omega_{L2}$, $\vec{k}_b = \vec{k}_{L1} - \vec{k}_{L2}$, $\phi_{pL} = eA_{L1}A_{L2}/2m_e\omega_{L1}\omega_{L2}$, $\vec{B}_{L1} = c\vec{k}_{L1} \times \vec{E}_{L1}/\omega_{L1}$ and $\vec{B}_{L2} = c\vec{k}_{L2} \times \vec{E}_{L2}/\omega_{L2}$. This ponderomotive force $\vec{F}_p$ drives a Langmuir wave (plasma beat wave) whose electrostatic potential can be given by $\phi_b = \phi_b e^{-i(\omega_b t-k_b z)}$. This wave is generated by the

https://doi.org/10.1017/S0263034607000511 Published online by Cambridge University Press

beating of above two lasers and is responsible for the OTSI. Therefore, it produces shorter wavelength Langmuir sideband waves (ω_1, k_1) and (ω_2, k_2) with $\omega_1 = \omega - \omega_b$, $\omega_2 = \omega + \omega_b$, $k_1 = k - k_b$, and $k_2 = k + k_b$, and low frequency electrostatic mode (ω, k) with $k > k_b$. The electrostatic potential of low frequency mode is given by $\phi = \phi e^{-i(\omega t - kz)}$ and those of sideband waves $\phi_1 = \phi_1\, e^{-i(\omega_1 t - k_1 z)}$ and $\phi_2 = \phi_2 e^{-i(\omega_2 t - k_2 z)}$. The potentials ϕ_1 and ϕ_2 give rise to the following oscillatory velocities of the electrons

$$v_1 = -\frac{ek_1}{m_e\omega_1}\phi_1 \quad \text{and} \quad v_2 = -\frac{ek_2}{m_e\omega_2}\phi_2. \tag{1}$$

The following electron density perturbation n_{e1} is produced by the ponderomotive force and self consistent potentials ϕ_{pL} and ϕ

$$n_{e1} = \frac{k^2}{4\pi e}\chi_e(\phi + \phi_{pL}). \tag{2}$$

By ignoring the ponderomotive force on the ions because it is smaller by the electron to ion mass ratio, the ion density perturbations are obtained as

$$n_{h1} = -\frac{k^2}{4\pi Z_h e}(\chi_h\phi),\ n_{c1} = -\frac{k^2}{4\pi Z_c e}(\chi_c\phi) \quad \text{and} \quad n_{n1} = \frac{k^2}{4\pi Z_n e}(\chi_n\phi). \tag{3}$$

In the above relations, the electron susceptibility $\chi_e = 2\omega_p^2/k^2 v_{th}^2$ for $\omega \ll kv_{th}$, positive ions susceptibilities $\chi_h = 2\omega_{ph}^2/k^2\ v_{thh}^2$ and $\chi_c = 2\omega_{pc}^2/k^2 v_{thc}^2$ for $\omega \ll kv_{thh,c}$, and negative ion susceptibility $\chi_n = 2\omega_{pn}^2/k^2 v_{thn}^2$ for $\omega \ll kv_{thn}$ together with $v_{th}(=\sqrt{T_e/m_e})$ and $v_{thj}(=\sqrt{T_j/m_j})$ as the thermal speeds of the electrons and ions, respectively, for $j = h, c, n$. The corresponding plasma frequencies are given by $\omega_p^2 = 4\pi n_{0e}e^2/m_e$ and $\omega_{pj}^2 = 4\pi n_{0j}Z_j^2 e^2/m_j$, where Z_j is the number of charge on the respective ion.

If $\varepsilon = 1 + \chi_e + \sum_{j=h,c,n}\chi_j$, then $\varepsilon\phi = -\chi_e\phi_{pL}$ is obtained from the Poisson's equation $\nabla^2\phi = 4\pi e(n_e + Z_n\ n_n - Z_h n_h - Z_c n_c)$ with the help of densities $n_e = n_{0e} + n_{e1}$ and $n_j = n_{0j} + n_{j1}$ together with $j = h,c,n$. Also, we may rewrite $n_{e1} = (k^2/4\pi e)\ \chi_e(1 + \sum_{j=h,c,n}\ \chi_j/\varepsilon)\phi_{pL}$ with the use of n_{e1}, n_{j1}, and $\varepsilon\phi = -\chi_e\phi_{pL}$. This density perturbation n_{e1} in conjunction with the oscillatory velocity v_b (due to ϕ_b or E_b) produces the following nonlinear density perturbations at (ω_1, k_1) and (ω_2, k_2)

$$n_1^{NL} = \left(\frac{\vec{k}_1\cdot\vec{v}_b^*}{2\omega_1}\right)n_{e1} = -\left[\frac{k^2\chi_e\left(1+\sum_{j=h,c,n}\chi_j\right)}{8\,m_e\pi i\omega_b\omega_1\left(1+\chi_e+\sum_{j=h,c,n}\chi_j\right)}\right] \times (\vec{k}_1\cdot\vec{E}_b^*)\phi_{pL}, \tag{4}$$

$$n_2^{NL} = \left(\frac{\vec{k}_2\cdot\vec{v}_b^*}{2\omega_2}\right)n_{e1} = -\left[\frac{k^2\chi_e\left(1+\sum_{j=h,c,n}\chi_j\right)}{8\,m_e\pi i\omega_b\omega_2\left(1+\chi_e+\sum_{j=h,c,n}\chi_j\right)}\right] \times \left(\vec{k}_2\cdot\vec{E}_b^*\right)\phi_{pL}. \tag{5}$$

Following linear density perturbations at the sidebands (ω_1, k_1) and (ω_2, k_2) are obtained

$$n_1^L = \frac{k^2}{4\pi e}\chi_{e1}\phi_1 \text{ and } n_2^L = \frac{k^2}{4\pi e}\chi_{e2}\phi_2, \tag{6}$$

where $\chi_{e1} = 2\omega_p^2/k_1^2\ v_{th}^2$ and $\chi_{e2} = 2\omega_p^2\ /k_2^2\ v_{th}^2$.

The use of Eqs. (4)–(6), i.e., the expressions of nonlinear and linear density perturbations, in the Poisson's equation yields

$$\varepsilon_1\phi_1 + \left[\frac{e^2k_b^2k^2}{4\,m_e^2\omega_b^2k_1\omega_1}\frac{\chi_e\left(1+\sum_{j=h,c,n}\chi_j\right)}{\left(1+\chi_e+\sum_{j=h,c,n}\chi_j\right)}\right] \times\left\{\left(\frac{k_1\phi_1}{\omega_1}\phi_b + \frac{k_2\phi_2}{\omega_2}\phi_b^*\right)\phi_b^*\right\} = 0, \tag{7}$$

$$\varepsilon_2\phi_2 + \left[\frac{e^2k_b^2k^2}{4\,m_e^2\omega_b^2k_2\omega_2}\frac{\chi_e\left(1+\sum_{j=h,c,n}\chi_j\right)}{\left(1+\chi_e+\sum_{j=h,c,n}\chi_j\right)}\right] \times\left\{\left(\frac{k_1\phi_1}{\omega_1}\phi_b + \frac{k_2\phi_2}{\omega_2}\phi_b^*\right)\phi_b\right\} = 0, \tag{8}$$

where $\varepsilon_1 = 1 - (\omega_p^2 + 3\,k^2v_{th}^2/2)/\omega_1^2$ and $\varepsilon_2 = 1 - (\omega_p^2 + 3\,k^2v_{th}^2/2)/\omega_2^2$. Now assuming the same velocities of the sidebands that is, $k_1/\omega_1 = k_2/\omega_2$ and defining $\delta = \omega_b - \sqrt{(\omega_p^2 + 3\,k^2v_{th}^2/2)}$, $\Omega = \omega_b\chi_e(1 + \sum_{j=h,c,n}\chi_j)/8(1 + \chi_e + \sum_{j=h,c,n}\chi_j)$ and $y_b = e\phi_b\,k_b^2/m_e\omega_b^2$, the following relations are obtained from the above equations

$$\left\{\omega - i\Gamma_1 - [\Omega|y_b|^2 + \delta]\right\}\phi_1 - \Omega y_b^{*2}\phi_2 = 0, \tag{9}$$

$$\Omega y_b^{*2}\phi_1 + \left\{\omega - i\Gamma_2 + [\delta + \Omega|y_b|^2]\right\}\phi_2 = 0. \tag{10}$$

Here Γ_1 and Γ_2 are the linear damping rates of the sideband waves, which may be attributed to the collisional or Landau damping in the parametric process. For $\Gamma_1 = \Gamma_2 = \Gamma$, the following dispersion relation is derived with the help of Eqs. (9) and (10)

$$\omega^2 - 2i\Gamma\omega - \delta^2 - \Omega^2|y_b|^4 - 2\delta\Omega|y_b|^2 + \Omega^2y_b^{*4} - \Gamma^2 = 0. \tag{11}$$

This relation reveals that the instability occurs when the frequency mismatch $\delta < 0$. Finally, the growth rate

https://doi.org/10.1017/S0263034607000511 Published online by Cambridge University Press

($\gamma_r = -i\omega$) of the instability is calculated as

$$\gamma_r = -\Gamma + \sqrt{-\delta(2\Omega|y_b|^2 + \delta)}. \quad (12)$$

Now this is clear here that the threshold for the instability is $|y_b|^2 \geq \Gamma/\Omega$, where $\Gamma \approx \nu_{ei}/2$ in a collisional plasma together with ν_{ei} as the electron-ion collision frequency.

3. PLASMA BEAT WAVE AND SIDEBAND WAVES

A nonlinear density perturbation n_b^{NL} at $(\omega_b, \vec{k}_b)$ is resulted from the combined effect of the density perturbation n_{e1} and the oscillating electron velocities $\vec{v}_1$ at (ω_1, k_1) and $\vec{v}_2$ at (ω_2, k_2). This is given by $n_b^{NL} = [\vec{k}_b \cdot (n_{e1}\vec{v}_1^* + n_{e1}^*\vec{v}_2)]/2\omega_b$, the use of which in the Poisson's equation gives rise to

$$\chi_{eb}\phi_{pL} + (1+\chi_{eb})\phi_b + \frac{4\pi e}{2\omega_b k^2}[\vec{k}_b \cdot (n_{e1}\vec{v}_1 * + n_{e1}^*\vec{v}_2)] = 0. \quad (13)$$

Here $\chi_{eb} = -(\omega_p^2 + 3\,k^2\,v_{th}^2/2)/\omega_b^2$ at frequency ω_b. The first term occurring in the above equation drives the plasma wave. Further, Eq. (13) takes the following form along with $1 + \chi_{eb} = \varepsilon_b$

$$\chi_{eb}\phi_{pL} + \varepsilon_b\phi_b + \left[\frac{e^2k^2\omega_1^2k_b^2\chi_e(1+\sum_{j=h,c,n}\chi_j)}{4m_e^2\omega_b^2\omega_p^2k_1^2(1+\chi_e+\sum_{j=h,c,n}\chi_j)}\right] \times \left\{\begin{array}{l}\left(\frac{k_1^2}{\omega_1^2}\phi_1\phi_1^* + \frac{k_2^2}{\omega_2^2}\phi_2\phi_2^*\right)\phi_b \\ +\left(\frac{2k_1k_2}{\omega_1\omega_2}\phi_2\phi_1^*\right)\phi_b^*\end{array}\right\} = 0. \quad (14)$$

Now $[\chi_e(1+\sum_{j=h,c,n}\chi_j)/(1+\chi_e+\sum_{j=h,c,n}\chi_j)]$ is taken as β, ω_b is replaced by $\omega_b + i\partial/\partial t$ and the Taylor expansion of $\varepsilon_b(\omega_b, k_b)$ is used around t = 0. This way one can express $\varepsilon_b(\omega_b, k_b) = -i(\partial\varepsilon_b/\partial\omega_b)\partial/\partial t$, where $\varepsilon_b(\omega_b, k_b)_{t=0} \ll \partial\varepsilon_b(\omega_b, k_b)/\partial\omega_b$, and obtains

$$i\frac{\omega_b}{2}\phi_{pL} + \frac{\partial\phi_b}{\partial t} - i\left(\frac{e^2k^2\omega_1^2k_b^2}{4m_e^2\omega_b^2\omega_p^2k_1^2}\right)\left[\left(\frac{k_1^2}{\omega_1^2}\phi_1\phi_1^* + \frac{k_2^2}{\omega_2^2}\phi_2\phi_2^*\right)\phi_b + \left(\frac{2k_1k_2}{\omega_1\omega_2}\phi_2\phi_1^*\right)\phi_b^*\right]\frac{\beta}{(\partial\varepsilon_b/\partial\omega_b)} = 0. \quad (15)$$

Similar approach gives the following from Eqs. (7) and (8)

$$\frac{\partial\phi_1}{\partial t} + i\left(\frac{e^2k^2k_b^2\omega_1}{4m_e^2\omega_b^3k_1}\right)\left[\left(\frac{k_1\phi_1}{\omega_1}\phi_b + \frac{k_2\phi_2}{\omega_2}\phi_b^*\right)\phi_b^*\right] \times \frac{\beta}{(\partial\varepsilon_1/\partial\omega_1)\gamma_r} = 0, \quad (16)$$

$$\frac{\partial\phi_2}{\partial t} - i\left(\frac{e^2k^2k_b^2\omega_2}{4m_e^2\omega_b^3k_2}\right)\left[\left(\frac{k_1\phi_1}{\omega_1}\phi_b + \frac{k_2\phi_2}{\omega_2}\phi_b^*\right)\phi_b\right]\frac{\beta}{(\partial\varepsilon_2/\partial\omega_2)\gamma_r} = 0. \quad (17)$$

Now Eqs. (15)–(17) are reduced in non-dimensional form with the help of normalization of the quantities ϕ_b, ϕ_1, ϕ_2, ϕ_{pL}, ω_b, t, γ_r, δ and Ω as $e\phi_b/T_e = Y_b$, $e\phi_1/T_e = Y_1$, $e\phi_2/T_e = Y_2$, $e\phi_{pL}/T_e = Y_{pL}$, $\omega_b/\omega_{pi} = \Omega_b$, $\omega_{pi}\,t = t'$, $\gamma_r/\omega_{pi} = \gamma_0$, $\delta/\omega_{pi} = \delta_0$, $\Gamma/\omega_{pi} = \Gamma_0$ and $\Omega/\omega_{pi} = \Omega_{bb}$. Then above equations read

$$\frac{\partial Y_b}{\partial t'} + i\frac{k^2k_b^2T_e^2}{8\omega_{ph}m_e^2\omega_p^2}\left[\frac{Y_1Y_1^*Y_b + Y_2Y_2^*Y_b + 2Y_2Y_1^*Y_b^*}{\chi_{eb}\omega_b\beta^{-1}}\right] + \frac{i\Omega_bY_{pL}}{2} = 0, \quad (18)$$

$$\frac{\partial Y_1}{\partial t'} - i\frac{k^2k_b^2T_e^2\omega_1^3}{8\omega_{ph}^2m_e^2\gamma_0\omega_b^3}\left[\frac{Y_1Y_bY_b^* + Y_2Y_b^{*^2}}{\chi_{eb}\omega_b^2\beta^{-1}}\right] = 0, \quad (19)$$

$$\frac{\partial Y_2}{\partial t'} + i\frac{k^2k_b^2T_e^2\omega_2^2}{8\omega_{ph}^2m_e^2\gamma_0\omega_b^3}\left[\frac{Y_1Y_b^2 + Y_2Y_b^*Y_b}{\chi_{eb}\omega_b^2\beta^{-1}}\right] = 0. \quad (20)$$

Now taking $Y_b = y_b(t')e^{i\varphi_b(t')}$, $Y_1 = y_1(t')e^{i\varphi_1(t')}$, $Y_2 = y_2(t')e^{i\varphi_2}(t')$ and $Y_{pL} = y_{pL}(t')e^{i\varphi_{pL}}(t')$ in Eqs. (18)–(20) the real and imaginary parts are separated out, which yields

$$\frac{\partial y_b}{\partial t'} + 2y_by_1y_2\left(\frac{\omega_b}{4\omega_{ph}}\right)\left(\frac{kv_{th}}{\omega_p}\right)^2\left(\frac{k_bv_{th}}{\omega_p}\right)^2 \times \left[\frac{\beta}{2+3(kv_{th}/\omega_p)^2}\right]\sin(\varphi_2 - \varphi_1 - 2\varphi_b) + \frac{\Omega_by_{pL}}{2}\sin(\varphi_b - \varphi_{pL}) = 0, \quad (21)$$

$$\frac{\partial y_1}{\partial t'} + y_2y_b^2\left(\frac{\omega_p^2}{4\omega_{ph}^2\gamma_0}\right)\left(\frac{\omega_1}{\omega_b}\right)^3\left(\frac{kv_{th}}{\omega_p}\right)^2\left(\frac{k_bv_{th}}{\omega_p}\right)^2\left[\frac{\beta}{2+3(kv_{th}/\omega_p)^2}\right] \times \sin(\varphi_2 - \varphi_1 - 2\varphi_b) = 0, \quad (22)$$

$$\frac{\partial y_2}{\partial t'} - y_1y_b^2\left(\frac{\omega_p^2}{4\omega_{ph}^2\gamma_0}\right)\left(\frac{\omega_2}{\omega_b}\right)^3\left(\frac{kv_{th}}{\omega_p}\right)^2\left(\frac{k_bv_{th}}{\omega_p}\right)^2\left[\frac{\beta}{2+3(kv_{th}/\omega_p)^2}\right] \times \sin(\varphi_2 - \varphi_1 - 2\varphi_b) = 0, \quad (23)$$

$$\frac{\partial\varphi_b}{\partial t'} - \left(\frac{\omega_b}{4\omega_{ph}}\right)\left(\frac{kv_{th}}{\omega_p}\right)^2\left(\frac{k_bv_{th}}{\omega_p}\right)^2 \times \left[\frac{\beta}{2+3(kv_{th}/\omega_p)^2}\right]\{y_1^2 + y_2^2 + 2y_1y_2\cos(\varphi_2 - \varphi_1 - 2\varphi_b)\} + \left(\frac{\Omega_by_{pL}}{2y_b}\right)\cos(\varphi_b - \varphi_{pL}) = 0, \quad (24)$$

https://doi.org/10.1017/S0263034607000511 Published online by Cambridge University Press

$$\frac{\partial\varphi_1}{\partial t'} - y_b^2\left(\frac{\omega_p^2}{4\omega_{ph}^2\gamma_0}\right)\left(\frac{\omega_1}{\omega_b}\right)^3\left(\frac{kv_{th}}{\omega_p}\right)^2\left(\frac{k_b v_{th}}{\omega_p}\right)^2 \times\left[\frac{\beta}{2+3(kv_{th}/\omega_p)^2}\right]\left\{1+\frac{y_2}{y_1}\cos(\varphi_2-\varphi_1-2\varphi_b)\right\}=0, \quad (25)$$

$$\frac{\partial\varphi_2}{\partial t'} - y_b^2\left(\frac{\omega_p^2}{4\omega_{ph}^2\gamma_0}\right)\left(\frac{\omega_2}{\omega_b}\right)^3\left(\frac{kv_{th}}{\omega_p}\right)^2\left(\frac{k_b v_{th}}{\omega_p}\right)^2 \times\left[\frac{\beta}{2+3(kv_{th}/\omega_p)^2}\right]\left\{1+\frac{y_1}{y_2}\cos(\varphi_2-\varphi_1-2\varphi_b)\right\}=0. \quad (26)$$

In these equations, $\gamma_0 = \left[\Omega_{bb}^2|(k_b^2T_e/m_e\omega_b^2)Y_b|^4 - \times\left(\delta_0+\Omega_{bb}|(k_b^2T_e/m_e\omega_b^2)Y_b|^2\right)^2\right]^{1/2} - \Gamma_0$.

4. RESULTS AND DISCUSSION

The coefficient $\beta = [\chi_e(1+\sum_{j=h,c,n}\chi_j)/(1+\chi_e+\sum_{j=h,c,n}\chi_j)]$ can be written in the following form

$$\beta = \left[1+\frac{1}{k^2\lambda_{de}^2}\sum_{j=h,c,n}\frac{n_{je}}{T_{je}}Z_j^2\right]/\left[1+k^2\lambda_{de}^2+\sum_{j=h,c,n}\frac{n_{je}}{T_{je}}Z_j^2\right], \quad (27)$$

where $n_{je} = n_{0j}/n_{0e}$ and $T_{je} = T_j/T_e$ for $j = h,c,n$. Clearly it depends on the density, temperature and charge number of the positive and negative ions. Also, this coefficient β appears in the expressions of the growth rate via Ω [Eq. (12)] and the amplitudes y_b, y_1 and y_2, and the phases φ_b, φ_1 and φ_2 [Eqs. (21)–(26)]. Therefore, the positive and negative ions have direct influence on the growth rate of the instability and the sideband waves generated during the OTSI.

Since the OTSI is the problem related to the particle acceleration, which is focused to contribute towards the fusion research, and alpha particles contribute to the continuous plasma burning in nuclear fusion reactors of deuterium-tritium reaction, helium hydrogen plasma seems to be important for discussing this instability. Moreover, in such a laser plasma interaction, the laser energy gets transferred to the plasma and there is a great possibility of generation of different types of ions, viz. positive and negative ions of different temperatures. Therefore, in the present calculations, the plasma is considered to have positive (negative) helium ions and negative (positive) hydrogen ions with two temperature distribution of positive ions.

4.1. Growth rate

The normalized growth rate $\Gamma_p = \gamma_r + \Gamma$ is analyzed in this section with the help of various figures for a helium hydrogen plasma with positive (negative) helium ions and negative (positive) hydrogen ions. Figure 1 shows the weak dependence of Γ_p on hot ion to electron temperature ratio T_{he} and the density ratio n_{he} (or n_{ne}) in the plasma having different species like (H_e^+, H^-) and (H_e^{++}, H^-), when $n_{0e} = 1\times10^{22}/m^3$, $T_e = 500$ eV, $T_c = T_n = T_h/100$, $n_{ce} = 0.9$ and $\omega_b = 0.99\omega_p$. Solid (dotted) line graphs $\Gamma p1$ ($\Gamma p2$) stand for $Z_h = Z_c = 1$ (2).

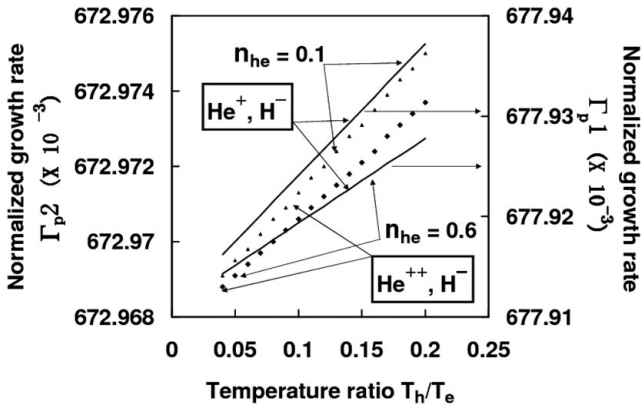

Fig. 1. Dependence of normalized growth rate Γ_p on hot ion to electron temperature ratio for two different values of n_{he} and the charge number Z_j (for $He^{+/++}$, H^- ions), when $n_{0e} = 1\times10^{22}/m^3$, $T_e = 500$ eV, $T_c = T_n = T_h/100$, $n_{ce} = 0.9$ and $\omega_b = 0.99\omega_p$. Solid (dotted) line graphs $\Gamma p1$ ($\Gamma p2$) stand for $Z_h = Z_c = 1$ (2).

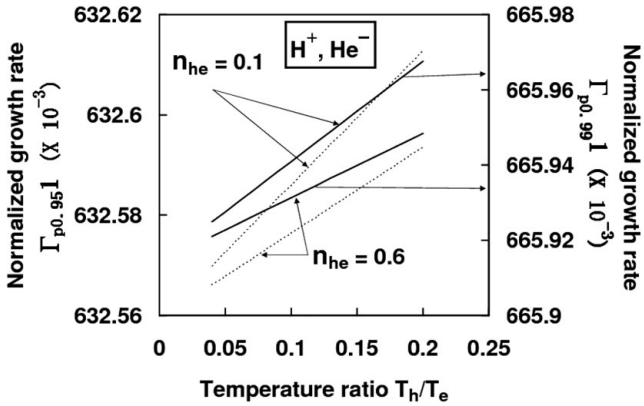

Fig. 2. Dependence of normalized growth rate Γ_p on hot ion to electron temperature ratio for two different values of n_{he} in a plasma having He^- and H^+ ions for $Z_h = Z_c = 1$ and the same parameters as in Figure 1. Here $\Gamma_{p0.95}1$ ($\Gamma_{p0.99}1$) stands for $\omega_b = 0.95\omega_p$ ($0.99\omega_p$).

https://doi.org/10.1017/S0263034607000511 Published online by Cambridge University Press

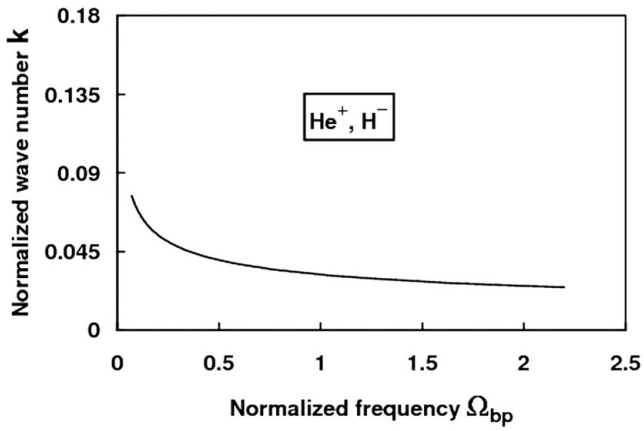

Fig. 3. Dependence of normalized wave number k on the normalized frequency Ω_{bp} in a plasma having He^+ and H^- ions, when $n_{0e} = 1 \times 10^{22}/m^3$, $T_e = 500$ eV, $T_h = T_e/5$, $T_c = T_n = T_h/100$, $n_{ce} = 0.9$, $n_{he} = 0.6$, $n_{ne} = 0.5$, $k/k_b = 6$ and $\omega_b = 0.99\omega_p$.

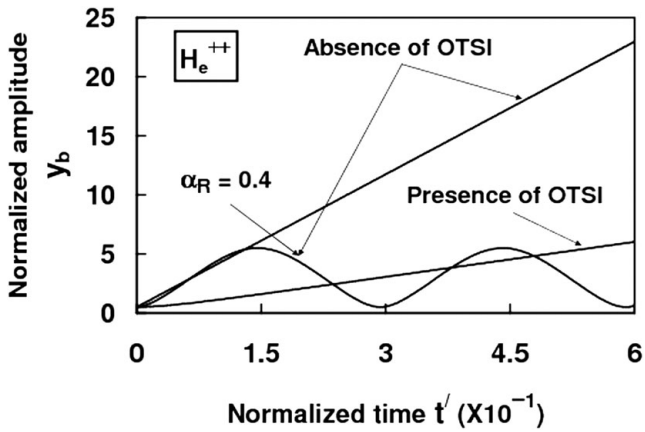

Fig. 5. Temporal evolution of the normalized pump wave amplitude y_b in a plasma having He^{++} and H^- ions, when $n_{0e} = 1 \times 10^{22}/m^3$, $n_{ce} = 0.9$, $n_{he} = 0.6$, $n_{ne} = 2.0$, $T_e = 500$ eV, $T_h = T_e/5$, $T_c = T_n = T_h/100$, $k_b v_{th}/\omega_p = 0.1$, $k/k_b = 3$, $\Omega_b y_{pL}/2 = 10$, $\varphi_{pL} = 0$, $\Gamma_0 = 2.5$ and $\omega_b = 0.99\omega_p$.

instability in this type of plasma is comparatively slower. Therefore, the effect of mass of positive ions m_h (or m_c) is to increase the growth rate. However, an opposite effect of mass of negative ions is obtained on Γ_p. Moreover, a comparison between the graphs for $\Gamma_{p0.95}1$ (dotted lines, where $\omega_b = 0.95\omega_p$) and $\Gamma_{p0.99}1$ (solid lines, where $\omega_b = 0.99\omega_p$) shows that the growth rate is larger for the case of $\omega_b = 0.99\omega_p$ in comparison to the case of $\omega_b = 0.95\omega_p$. This increased growth rate is attributed to the frequency mismatch δ.

Figure 3 shows the change in wave number k of the low frequency electrostatic mode with the normalized frequency $\Omega_{bp} = (\omega_b/8)2\omega_p^2/\{(6\,k_b)^3 v_{th}^3 (m_e/m_h)^{1/2}\}$ when $k_b v_{th}/\omega_p$ ranges from 0.35 to 1.1. This is evident from this figure that the wave number k is sensitive to the frequency (or wave number) of the laser driven plasma beat wave. However, in Figure 4, when we make a comparative study of the variation of k in (He^+, H^-) and (He^-, H^+) plasmas, we realize that the wave number k is more sensitive in the plasma having lighter positive ions.

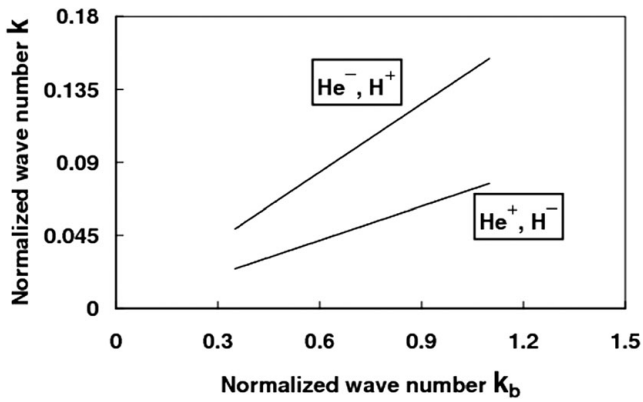

Fig. 4. Dependence of normalized wave number k on the normalized wave number k_b in a plasma having He^+ and H^- ions or He^- and H^+ ions for the same parameters as in Figure 3.

4.2. Pump wave amplitude

In order to study the temporal evolution of the amplitudes of pump wave and sideband waves generated during the OTSI, the coupled Eq. (21)–(26) are solved by Runga-Kutta method, using the normalized parameters (Gupta *et al.*, 2004) as $k_b v_{th}/\omega_p = 0.1$, $k_b/k = 0.3$, $\Omega_b y_{pL}/2 = 10$, $\varphi_{pL} = 0$, $\delta_0 = -0.24$, $\Omega_{bb} = 0.2$, $\Gamma_0 = 2.5$, $\varphi_b = \varphi_1 = 0$, $\varphi_2 = \pi/2$, $\omega_b = 0.99\omega_p$, $y_b = 0.5$, $y_1 = y_2 = 0.01$ at the initial time $t' = 0$. Figure 5 shows the evolution of the amplitude $y_b = e\phi_b/T_e$ in the presence of the OTSI as well as in its absence in a plasma having singly charged negative hydrogen ions and doubly charged helium positive ions. Here it is clear that the amplitude y_b gets reduced in the presence of the OTSI, as the energy is diverted to the sidebands y_1 and y_2. Since the oscillatory electron velocity due to the Langmuir wave is larger than v_{L1} and v_{L2}, the relativistic mass correction due to v_{L1} and v_{L2} was neglected in the calculations. However, the following is obtained for φ_b along with the relativistic correction $\alpha_R = 3e^2k_b^2/16\omega_b(m_e c)^2$

$$\frac{\partial \varphi_b}{\partial t'} - \left(\frac{\omega_b}{4\omega_{ph}}\right)\left(\frac{kv_{th}}{\omega_p}\right)^2\left(\frac{k_b v_{th}}{\omega_p}\right)^2\left[\frac{\beta}{2+3(kv_{th}/\omega_p)^2}\right] \times \{y_1^2 + y_2^2 + 2y_1y_2\cos(\varphi_2 - \varphi_1 - 2\varphi_b)\} + \left(\frac{\Omega_b y_{pL}}{2y_b}\right)\cos(\varphi_b - \varphi_{pL}) - \alpha_R y_b^2 = 0. \quad (28)$$

With the above expression of φ_b, the time evolution of y_b in Figure 5 shows that it has oscillating nature, as seen in the case of ordinary plasma having positive ions and electrons (Gupta *et al.*, 2004).

4.3. Sideband waves

In this section, the effects of charge number, mass and density of ions will be examined on the temporal evolution

https://doi.org/10.1017/S0263034607000511 Published online by Cambridge University Press

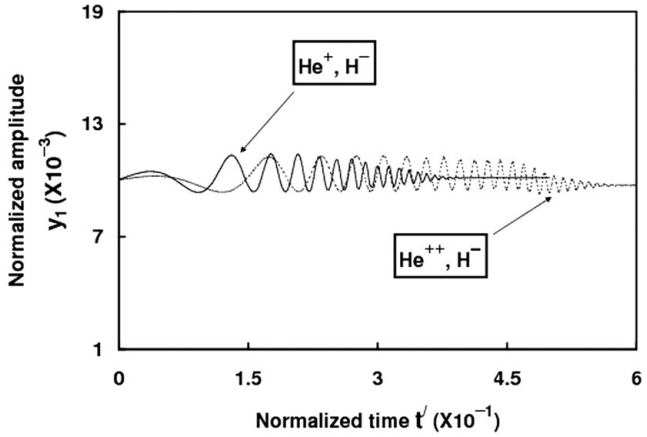

Fig. 6. Temporal evolution of the normalized amplitude y_1 of the sideband wave in a plasma having singly ($n_{ne} = 0.5$) or doubly ($n_{ne} = 2.0$) charged helium ions, showing the effect of charge number Z_j for the same parameters as in Figure 5.

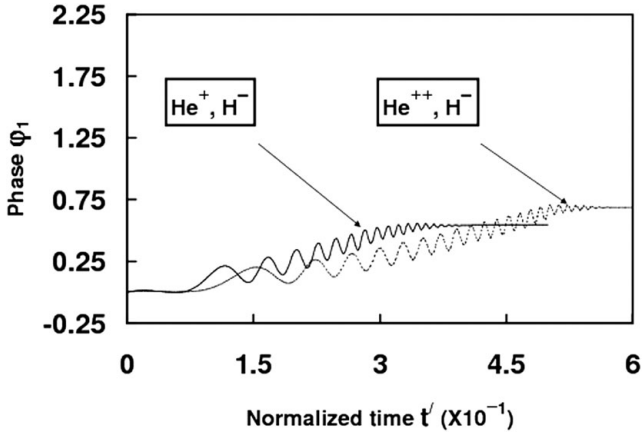

Fig. 8. Temporal evolution of the phase φ_1 of the sideband wave corresponding to Figure 6.

of the amplitudes y_1 and y_2, and the phases φ_1 and φ_2 of the sideband waves.

4.3.1. Effect of charge number Z_j

Figures 6 and 7 show the temporal evolution of the amplitudes y_1 and y_2 of the sideband waves for two different values of charge number Z_h ($=Z_c$) of the helium ions. In these figures, the dotted line graphs represent the case of higher charge number ($Z_j = 2$). The figures demonstrate that the amplitudes of both the sideband waves maintain comparatively higher amplitude for longer duration in the plasma having ions of higher Z_j, and the magnitude of the amplitude y_2 at (ω_2, k_2) is larger than that of y_1 at (ω_1, k_1). This variation of amplitudes is in accordance with the dependence of growth rate Γ_p on Z_j in Figure 1: since the growth Γ_p is comparatively lower for the case of larger Z_j, the low frequency electrostatic mode (ω, k) gains lower energy from the plasma beat wave. Hence, more energy is coupled to the sideband waves that lead to their larger amplitudes for longer duration. In addition, the temporal evolution of the corresponding phases φ_1 and φ_2 of the sidebands in Figures 8 and 9 shows that the change in the phases is more significant in the plasma having ions of higher charge number Z_j.

4.3.2. Effect of ion mass m_j

The temporal evolution and variation of the amplitudes y_1 and y_2 with the mass m_j of positive and negative ions is shown in Figures 10 and 11, respectively, where y_1 and y_2 are sketched in the plasma having either He^+ and H^- ions or H^+ and He^- ions. In these figures, the solid line curves are for H^- (or He^+) ions whereas the dotted line curves are for the case of He^- (or H^+) ions. Therefore, a comparison of the solid line graphs with the dotted ones yields that both the amplitudes y_1 and y_2 maintain their higher amplitude for longer duration in the plasma having lighter positive or heavier negative ions. This behavior of the amplitudes can be explained with the help of Figures 1 and 2, which show that the growth rate is smaller in the plasma having lighter

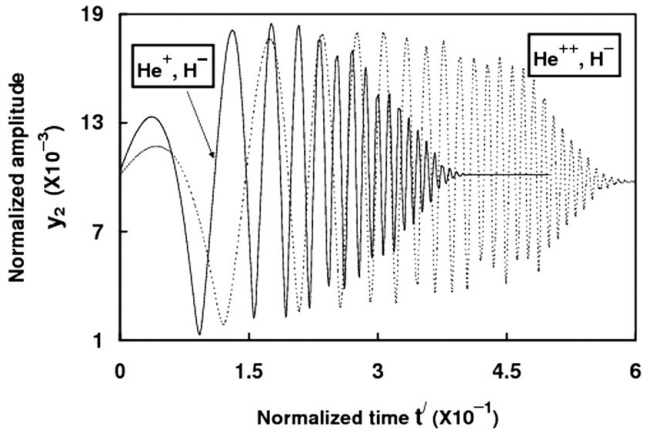

Fig. 7. Temporal evolution of the normalized amplitude y_2 of the sideband wave in plasma having singly or doubly charged helium ions, showing the effect of charge number Z_j for the same parameters as in Figure 6.

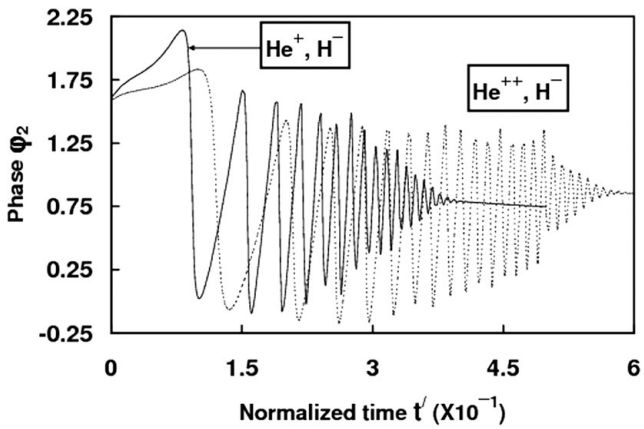

Fig. 9. Temporal evolution of the phase φ_2 of the sideband wave corresponding to Figure 7.

https://doi.org/10.1017/S0263034607000511 Published online by Cambridge University Press

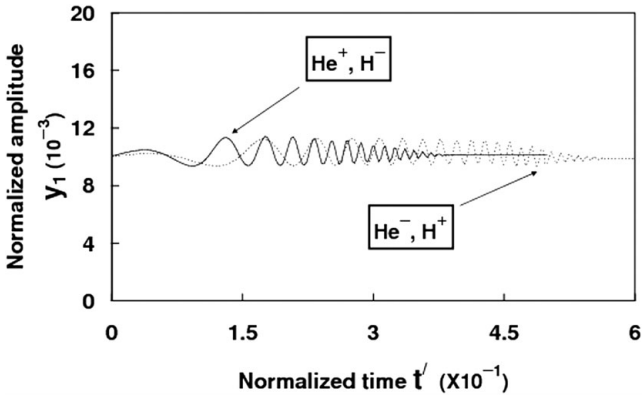

Fig. 10. Temporal evolution of the normalized amplitude y_1 of the sideband wave in a plasma having He^+ and H^- ions or He^- and H^+ ions, showing the effect of ion mass m_j for the same parameters as in Figure 6.

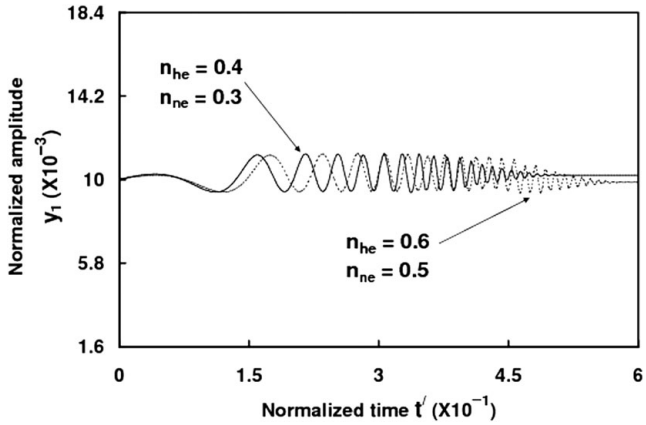

Fig. 12. Temporal evolution of the normalized amplitude y_1 of the sideband wave in plasma having He^- and H^+ ions, showing the effect of ion density n_{je} for the same parameters as in Figure 6.

positive ions. This way lower energy is coupled to the mode (ω, k) and more energy is diverted to the sidebands. Therefore, this will cause the larger amplitudes of the sideband waves.

4.3.3. Effect of density of ions n_{0j}

The behavior of the amplitudes and corresponding phases of the sidebands with positive ion to electron density ratio $n_{he} \equiv n_{0h}/n_{0e}$ or negative ion to electron density ratio $n_{ne} \equiv n_{0n}/n_{0e}$ (which is evident from the charge neutrality condition $Z_h\, n_{0h} + Z_c\, n_{0c} = n_{0e} + Z_n\, n_{0n}$ or $Z_h\, n_{0h}/n_{0e} + Z_c n_{0c}/n_{0e} = 1 + Z_n n_{0n}/n_{0e}$) is displayed in Figures 12–15 for a plasma having He^- and H^+ ions. From these figures one may note that the amplitudes maintain higher magnitudes for longer duration for the case of larger density n_{he} (n_{ne}) of positive (negative) ions, which is consistent with the variation of growth rate with n_{he} (n_{ne}) (Fig. 1). Also, the variation of phases φ_1 and φ_2 of the sideband waves is in accordance with the amplitudes. On the other hand, the present calculations infer that the effect of ion temperature on the amplitudes and phases is opposite to the ones of density and charge number of the positive ions.

5. CONCLUDING REMARKS

The present analysis models an oscillating two stream instability of a laser driven plasma beat wave in a plasma that has hot and cold positive ions, negative ions, and the electrons. The simulation results infer that the growth rate shows weak dependence on the negative and positive ion density and their temperatures. However, the effect of charge number and mass of the ions is significant on the instability: growth rate gets reduced for the case of larger Z_j but it gets increased for the higher mass of the positive ions. Further, the wave number k of the low frequency electrostatic mode was found to be more sensitive to the frequency and wave number of the beat wave in plasma having lighter positive ions. The amplitudes of the sideband waves oscillate with higher magnitude for longer duration in

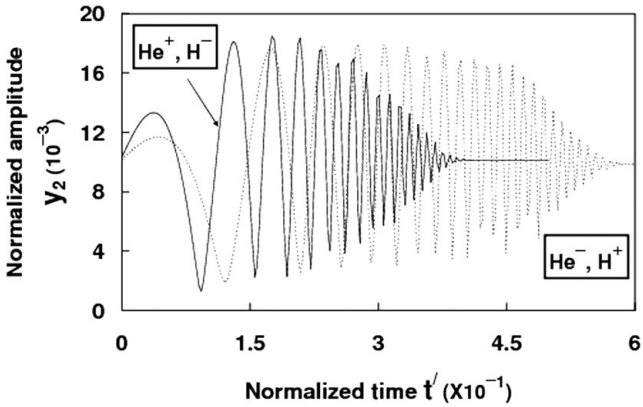

Fig. 11. Temporal evolution of the normalized amplitude y_2 of the sideband wave in a plasma having He^+ and H^- ions or He^- and H^+ ions, showing the effect of ion mass m_j for the same parameters as in Figure 6.

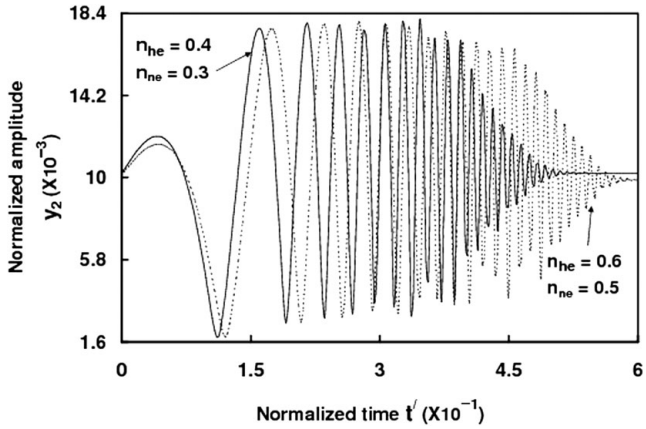

Fig. 13. Temporal evolution of the normalized amplitude y_2 of the sideband wave in a plasma having He^- and H^+ ions, showing the effect of ion density n_{je} for the same parameters as in Figure 6.

https://doi.org/10.1017/S0263034607000511 Published online by Cambridge University Press

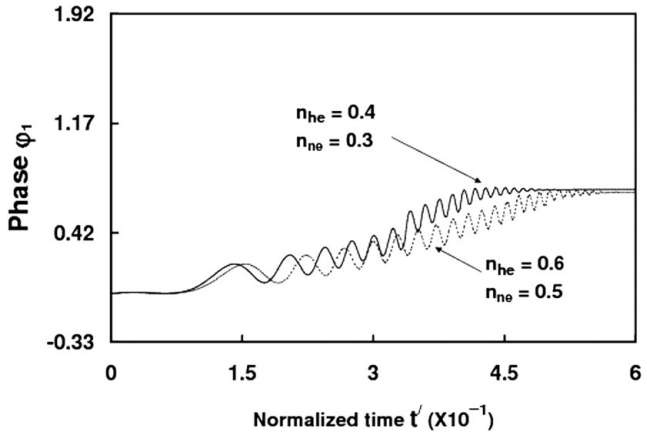

Fig. 14. Temporal evolution of the phase φ_1 of the sideband wave corresponding to Figure 12.

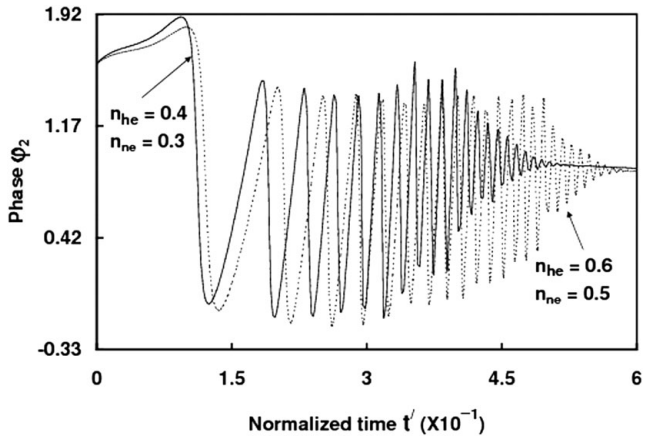

Fig. 15. Temporal evolution of the phase φ_2 of the sideband wave corresponding to Figure 13.

the plasma having lighter (heavier) positive (negative) ions and the ions of larger charge number. The densities of the negative and positive ions also affect the evolution of the sideband waves and similar effects are observed for the higher densities.

REFERENCES

Baiwen, L.I., Ishiguro, S., Skoric, M.M., Takamaru, H. & Sato, T. (2004). Acceleration of high-quality, well-collimated return beam of relativistic electrons by intense laser pulse in a low-density plasma. *Laser Part. Beams* **22**, 307–314.

Balakirev, V.A., Karas, V.I., Karas, I.V. & Levchenko, V.D. (2001). Plasma wake-field excitation by relativistic electron bunches and charged particle acceleration in the presence of external magnetic field. *Laser Part. Beams* **19**, 597–604.

Barnard, J.J., Ahle, L.E., Bieniosek, F.M., Celata, C.M., Davidson, R.C., Henestroza, E., Friedman, A., Kwan, J.W., Logan, B.G., Lee, E.P., Lund, S.M., Meier, W.R., Sabbi, G.L., Seidl, P.A., Sharp, W.M., Shuman, D.B., Waldron, W.L., Qin, H. & Yu, S.S. (2003). Integrated experiments for heavy ion fusion. *Laser Part. Beams* **21**, 553–560.

Blazquez, J.F.M. (2002). Application of solitons to the study of laser propagation into a thermonuclear plasma in inertial confinement fusion. *Laser Part. Beams* **20**, 153–157.

Bret, A. & Deutsch, C. (2006). Density gradient effects on beam plasma linear instabilities for fast ignition scenario. *Laser Part. Beams* **24**, 269–273.

Bret, A., Firpo, M.C. & Deutsch, C. (2005). Bridging the gap between two stream and filamentation instabilities. *Laser Part. Beams* **23**, 375–383.

Bret, A., Firpo, M.C. & Deutsch, C. (2006). Between two stream and filamentation instabilities: Temperature and collisions effects. *Laser Part. Beams* **24**, 27–33.

Bret, A., Firpo, M.C. & Deutsch, C. (2007). About the most unstable modes encountered in beam plasma interaction physics. *Laser Part. Beams* **25**, 117–119.

Davidson, R.C., Kaganovich, I.D., Lee, W.W., Qin, H., Startsev, E.A., Tzenov, S., Friedma, A., Barnard, J.J., Cohen, R.H., Grote, D.P., Lund, S.M., Sharp, W.M., Celata, C.M., Hoon, M.D., Henestroza, E., Lee, E.P., Yu, S.S., Vay, J.L., Welch, D.R., Rose, D.V. & Olson, C.L. (2002). Overview of theory and modeling in the heavy ion fusion virtual national laboratory. *Laser Part. Beams* **20**, 377–384.

Fernandez, J.C., Cobble, J.A., Failor, B.H., DuBois, D.F., Montgomery, D.S., Rose, H.A., Vu, H.X., Wilde, B.H., Wilke, M.D. & Chrien, R.E. (1996). Observed dependence of stimulated Raman scattering on ion-acoustic damping in hohlraum plasmas. *Phys. Rev. Lett.* **77**, 2702–2705.

Flippo, K., Hegelich, B.M., Albright, B.J., Yin, L., Gautier, D.C., Letzring, S., Schollmeier, M., Schreiber, J., Schulze, R. & Fernandez, J.C. (2007). Laser-driven ion accelerators: Spectral control, monoenergetic ions and new acceleration mechanisms. *Laser Part. Beams* **25**, 3–8.

Gupta, D.N., Singh, K.P., Sharma, A.K. & Jaiman, A.K. (2004). Nonlinear saturation of laser driven plasma beat wave by oscillating two-stream instability. *Phys. Plasmas* **11**, 5250–5255.

Gupta, D.N. & Suk, H. (2007). Electron acceleration to high energy by using two chirped lasers. *Laser Part. Beams* **25**, 31–36.

Hoffmann, D.H.H., Blazevic, A., Ni, P., Rosmej, O., Roth, M., Tahir, N.A., Tauschwitz, A., Udrea, S., Varentsov, D., Weyrich, K. & Maron, Y. (2005). Present and future perspectives for high energy density physics with intense heavy ion and laser beams. *Laser Part. Beams* **23**, 47–53.

Hora, H. (2004). Developments in inertial fusion energy and beam fusion at magnetic confinement. *Laser Part. Beams* **22**, 439–449.

Imasaki, K. & Li, D. (2007). An approach to hydrogen production by inertial fusion energy. *Laser Part. Beams* **25**, 99–105.

Joshi, C., Blue, B., Clayton, C.E., Dodd, E., Huang, C., Marsh, K.A., Mori, W.B., Wang, S., Hogan, M.J., O'Connell, C., Siemann, R., Watz, D., Muggli, P., Katsouleas, T. & Lee, S. (2002). High energy density plasma science with an ultrarelativistic electron beam. *Phys. Plasmas* **9**, 1845–1855.

Katsouleas, T. (2004). Progress on plasma accelerators: From the energy frontier to tabletops. *Plasma Phys. Contr. Fusion* **46**, B575–B582.

Kawata, S., Kong, Q., Miyazaki, S., Miyauchi, K., Sonobe, R., Sakai, K., Nakajima, K., Masuda, S., Ho, Y.K., Miyanaga, N., Limpouch, J. & Andreev, A.A. (2005). Electron bunch

https://doi.org/10.1017/S0263034607000511 Published online by Cambridge University Press

acceleration and trapping by ponderomotive force of an intense short-pulse laser. *Laser Part. Beams* **23**, 61–67.

Kawata, S., Someya, T., Nakamura, T., Miyazaki, S., Shimizu, K. & Ogoyski, A.I. (2003). Heavy ion beam final transport through an insulator guide in heavy ion fusion. *Laser Part. Beams* **21**, 27–32.

Kilkenny, J.D., Alexander, N.B., Nikaroo, A., Steinman, D.A., Nobile, A., Bernat, T., Cook, R., Letts, S., Takagi, M. & Harding, D. (2005). Laser targets compensate for limitations in inertial confinement fusion drivers. *Laser Part. Beams* **23**, 475–482.

Kirkwood, R.K., MacGowan, B.J., Montgomery, D.S., Afeyan, B.B., Kruer, W.L., Moody, J.D., Estabrook, K.G., Back, C.A., Glenzer, S.H., Blain, M.A., Williams, E.A., Berger, R.L. & Lasinski, B.F. (1996). Effect of ion-wave damping on stimulated Raman scattering in high- z laser-produced plasmas. *Phys. Rev. Lett.* **77**, 2706–2709.

Koresheva, E.R., Osipov, I.E. & Aleksandrova, I.V. (2005). Free standing target technologies for inertial fusion energy: Target fabrication characterization and delivery. *Laser Part. Beams* **23**, 563–571.

Koyama, K., Adachi, M., Miura, E., Kato, S., Masuda, S., Watanabe, T., Ogata, A. & Tanimoto, M. (2006). Monoenergetic electron beam generation from a laser-plasma accelerator. *Laser Part. Beams* **24**, 95–100.

Kruer, W.L. (1987). *The Physics of Laser Plasma Interactions*. Reading, MA: Addison-Wesley.

Kumar, A., Gupta, M.K. & Sharma, R.P. (2006). Effect of ultra intense laser pulse on the propagation of electron plasma wave in relativistic and ponderomotive regime and particle acceleration. *Laser Part. Beams* **24**, 403–409.

Kumar, S. & Malik, H.K. (2006). Effect of negative ions on oscillating two stream instability of a laser driven plasma beat wave in a homogeneous plasma. *Phys. Scripta* **74**, 304–309.

Kumar, S., Malik, H.K. & Nishida, Y. (2006). Wakefield excitation and electron acceleration by triangular and sawtooth laser pulses in a plasma: An analytical approach. *Phys. Scripta* **74**, 525–530.

Kuzora, I.V., Kozlov, M.V., McKinstrie, C.J., Ovchinnikov, K.N., Silin, V.P., Uryupin, S.A. & Vagin, K.Y. (2001). Thresholds and spectra of SBS in plasmas with two species of ions. *Phys. Lett. A* **284**, 194–204.

Leon, P.T., Eliezer, S., Piera, M. & Martinez-Val, J.M. (2005). Inertial fusion features in degenerate plasmas. *Laser Part. Beams* **23**, 193–198.

Li, X.Z., Liu, B., Chen, S., Wei, Q.M. & Hora, H. (2004). Fusion cross-sections for inertial fusion energy. *Laser Part. Beams* **22**, 469–477.

Lifschitz, A.F., Faure, J., Glinec, Y., Malka, V. & Mora, P. (2006). Proposed scheme for compact GeV laser plasma accelerator. *Laser Part. Beams* **24**, 255–259.

Liu, C.S. & Kaw, P.K. (1976). *Advances in Plasma Physics*. New York: Wiley.

Mulser, P., Giulietti, A. & Vaselli, M. (1984). Quantitative explanation of oscillating two-stream and parametric decay instabilities in terms of wave pressure. *Phys. Fluids* **27**, 2035–2038.

Nakajima, K. (1996). Challenge to a tabletop high-energy laser wake-field accelerator. *Phys. Plasmas* **3**, 2169–2174.

Nejoh, Y.N. (1992). Modulational instability of relativistic ion-acoustic waves in a plasma with trapped electrons. *IEEE Trans. Plasma Sci.* **20**, 80–85.

Nicholson, D.R. (1981). Oscillating two-stream instability with pump of finite extent. *Phys. Fluids* **24**, 908–910.

Nishida, Y. & Sato, N. (1987). Observation of high-energy electrons accelerated by electrostatic waves propagating obliquely to a magnetic field. *Phys. Rev. Lett.* **59**, 653–656.

Nishida, Y. & Shinozaki, T. (1990). Resonant wave-particle interactions in $\vec{V}_p \times \vec{B}$ acceleration scheme. *Phys. Rev. Lett.* **65**, 2386–2389.

Nishikawa, K. (1968*a*). Parametric excitation of coupled waves I. General formulation. *J. Phys. Soc. Japan* **24**, 916–922.

Nishikawa, K. (1968*b*). Parametric excitation of coupled waves II. Parametric plasmon photon interaction. *J. Phys. Soc. Japan* **24**, 1152–1158.

Oron, D., Sadot, O., Srebro, Y., Rikanati, A., Yedvab, Y., Alon, U., Erez, L., Erez, G., Ben-Dor, G., Levin, L.A., Ofer, D. & Shvarts, D. (1999). Studies in the nonlinear evolution of the Rayleigh–Taylor and Richtmyer–Meshkov instabilities and their role in inertial confinement fusion. *Laser Part. Beams* **17**, 465–475.

Pajouh, H.H., Abbasi, H. & Shukla, P.K. (2004). Nonlinear interaction of a Gaussian intense laser beam with plasma: Relativistic modulational instability. *Phys. Plasmas* **11**, 5693–5703.

Perlado, J.M., Sanz, J., Velarde, M., Reyes, S., Caturla, M.J., Arevalo, C., Cabellos, O., Dominguez, E., Marian, J., Martinez, E., Mota, F., Rodriguez, A., Salvador, M. & Velarde, G. (2005). Activation and damage of fusion materials and tritium effects in inertial fusion reactors: Strategy for adequate irradiation. *Laser Part. Beams* **23**, 345–349.

Qin, H., Davidson, R.C., Startsev, E.A. & Lee, W.W.L. (2003). delta f simulation studies of the ion-electron two-stream instability in heavy ion fusion beams. *Laser Part. Beams* **21**, 21–26.

Reitsma, A.J.W. & Jaroszynski, D.A. (2004). Coupling of longitudinal and transverse motion of accelerated electrons in laser wakefield acceleration. *Laser Part. Beams* **22**, 407–413.

Rudraiah, N., Krishnamurthy, B.S., Jalaja, A.S. & Desai, T. (2004). Effect of a magnetic field on the growth rate of the Rayleigh–Taylor instability of a laser-accelerated thin ablative surface. *Laser Part. Beams* **22**, 29–33.

Sakai, K., Miyazaki, S., Kawata, S., Hasumi, S. & Kikuchi, T. (2006). High-energy-density attosecond electron beam production by intense short-pulse laser with a plasma separator. *Laser Part. Beams* **24**, 321–327.

Satya, Y.S., Jain, K.M., Guha, S. & Bose, M. (1985). Low-frequency modes in a two-species plasma. *J. Plasma Phys.* **34**, 247–258.

Starodubtsev, M., Hassan, M.K., Ito, H., Yugami, N. & Nishida, Y. (2004). Low-frequency sheath instability in a non-Maxwellian plasma with energetic ions. *Phys. Rev. Lett.* **92**. 045003/1–4.

Starodubtsev, M., Hassan, M.K., Ito, H., Yugami, N. & Nishida, Y. (2006). Low-frequency sheath instability stimulated by an energetic ion component. *Phys. Plasmas* **13**, 012103/1–7.

Umstadter, D. (2001). Review of physics and applications of relativistic plasmas driven by ultra-intense lasers. *Phys. Plasmas* **8**, 1174–1185.

Young, P.E., Foord, M.E., Maximov, A.V. & Rozmus, W. (1996). Stimulated brillouin scattering in multispecies laser-produced plasmas. *Phys. Rev. Lett.* **77**, 1278–1281.

https://doi.org/10.1017/S0263034607000511 Published online by Cambridge University Press